

A robust microgrid using an inverter with CCS-MPC control and resilient operation

Epsita Das¹, Ambarnath Banerji², Sujit K. Biswas³

¹Department of Electrical Engineering, Meghnad Saha Institute of Technology, Kolkata, India

²Department of Electrical Engineering, Narula Institute of Technology, Kolkata, India

³Department of Electrical Engineering, St. Thomas College of Engineering and Technology, Kolkata, India

Article Info

Article history:

Received Feb 22, 2023

Revised Jun 5, 2023

Accepted Jun 25, 2023

Keywords:

CCS-MPC

NARX ANN

Non-linear inverter model

Robust microgrid

Voltage regulation

ABSTRACT

Modern generation trend through renewable energy-based distributed energy resources has made microgrids an important part of the power system. Robust control of the inverter providing quality power has become an essential microgrid (MG) requirement. This paper proposes continuous control set model predictive control (CCS-MPC) on inverter for dynamic voltage regulation supplying reactive power to the load for a MG. The proposed method uses the terminal voltage magnitude, which reduces calculation time, sensor per phase, and the engagement burden of the controller. This paper applies a nonlinear VSI model and a series parallel structure nonlinear autoregressive exogenous (NARX) model of artificial neural network (ANN) to predict future output which CCS-MPC optimizes. The proposed VSI with CCS MPC is applied to a case study of a real system as a plug-and-play device. Simulation shows the satisfactory result of the proposed controller. The inverter control system has been made resilient to protect itself and automatically recover from faults on the DC and AC side, providing quality power to its local load when the fault has been removed.

This is an open access article under the [CC BY-SA](https://creativecommons.org/licenses/by-sa/4.0/) license.



Corresponding Author:

Epsita Das

Department of Electrical Engineering, Meghnad Saha Institute of Technology

Nazirabad, Anandapur Rd, Uchhepota, Kolkata, West Bengal-700150, India

Email: epsita@msit.edu.in

1. INTRODUCTION

The layout of the modern power network is changing day by day, with microgrid (MG.) and smart grid (SG) emerging as the cornerstones of the new trends in power systems. MG primarily relies on renewable energy sources (RES) and empowers societies to decrease energy dependency on the conventional grid system. RES using photovoltaic (PV) energy conversion to electricity makes solar inverters inevitable in MGs. However, critical loads and the absence of inertia make a MG susceptible to instability. The voltage source inverter (VSI), being the principal element of the source in the MG, can be controlled to improve these issues.

In this paper, a grid-connected MG is described, having industrial consumers. This paper studies a case of a real-time system where voltage is controlled through on-load tap changers. This technique is inadequate for voltage profile control, resulting in voltage dip and fluctuations. Dropping the voltage level below the reference value hampers industrial production. A new control method is proposed in this paper for voltage regulation without disturbing the above existing system. A plug-and-play PV inverter is connected to the point of common coupling (PCC) to maintain the voltage profile at the reference value under extreme loading conditions. The inverter has battery backup during the absence of the sun. It also supplies reactive power to improve the voltage profile. Exchange of reactive power requires only magnitude difference between system bus and inverter bus. This paper uses only one inverter to demonstrate the above control

action. Another problem with industrial processes is sudden power interruption due to faults. Here a fault-resilient arrangement is proposed by which the system can overcome short-time power interruption.

Inverter installation in a system needs an associated circuit where the controller is the primary component. Conventional systems rely on classical proportional (P) and integral (I) control action for inverter control in this respect. The scheme using PI controllers for reference current extraction in the d - q axes has been proposed [1]. A similar approach is observed in [2], [3]. The PI controller needs to be tuned initially during installation and also if the operating condition changes. Therefore, particle swarm optimization (PSO) based techniques to determine controller gain constants are applied for three phases in [2]. Therefore, the controllers need to find optimization of six parameters (K_p , K_i in all three phases) which imposes burden on the controller and also consumes time. Further, PSO can also be lost in a sub-optimal region producing vague results. To overcome this, blending ant colony optimization (ACO) and PSO is used to tune PI controllers [3]. This meta-heuristic method guarantees an optimum result but takes long time because the controller needs to solve ACO and PSO simultaneously at the beginning. A grid-coupled inverter scheme with additional battery backup is proposed [4], which can also perform during grid disconnection. The scheme also uses a PI controller. The grid-tied inverter is modelled using its RLC parameters, leading to a linear 2nd order transfer function. However, inverters use semiconductor devices and exhibit nonlinear characteristics in form of on-off, saturation, and dead zone. Thus, a simple linearized model leads to erroneous results. Several research on inverter control in the form of FACTS device are also reported in the literature to impose plug-and-play features in inverters. A particular port-controlled Hamiltonian (PCH) system and an input-output linearization tracking control strategy have been proposed [5]. It requires the realization of a storage function for the passivated system. The STATCOM structure has been modelled with PCH to apply the passivity theorem. However, authors first convert the system into an input affine system which may result in a weak minimum phase, making the system difficult to control. The sources in the microgrid are of small capacity and more susceptible to change than the conventional synchronous generators. Therefore, reactive power management is crucial. A fuzzy neural control algorithm is proposed [6] for active (P) and reactive (Q) power control during grid disruption. The power of neural networks for classification and pattern reorganization is used, which is not available with simple fuzzy logic. The adaptive neuro-fuzzy interference (ANFIS) technique is presented [7] for tuning PID controllers for active and reactive power compensation through solar-inverter. Four sets of proportional, integral and derivative control coefficients need to be tuned in voltage and current control loops, making the system cumbersome. An observer is the state model where available measurements are taken as inputs and estimates the states as outputs. Observer-perceived methods for grid-connected inverter operation are described [8], where L and R values for the state and disturbance observer need to be tuned, restricting the device for plug-and-play use. A maximum power point tracking (MPPT) controlled 1-phase grid-tied inverter design aspect is demonstrated [9] to transfer solar energy to the grid. The least mean mixed norm control algorithm for the VSI is described [10] for real power extraction from the photovoltaic panel and also reactive and harmonic demand compensation of the load.

Predictive control predicts the future output considering previous details of a system or process and forecasting future input. A predictive deadbeat-controlled inverter supplies a doubly fed induction generator as proposed in [11]. Deadbeat controllers perform well without overshoot but are comparatively slower than model predictive control (MPC) [12]. MPC is also popular in literature because of its ability to predict a system's dependent variable from the measure of independent variables. An observer-recognized (MPC) [13] is used for grid voltage measurement to reduce the offset. MPC is also an important method for operating grid-connected inverters [14]. A droop-controller assisted with the MPC technique is proposed [15] to reduce voltage variation in the wind farm. A finite control set (FCS) MPC-driven grid-connected inverter switching is also presented [16], [17]. FCS-MPC does not require any modulator, yet complex calculations lead to variable switching of the inverter. An increased number of switching states cause harmonic penetration in voltage and current waveform, leading to power loss, and audible noise. The authors use three-phase control, which needs tuning of coefficients of three phases [18]. A continuous control set (CCS) MPC requires modulator but produce fixed switching frequency. A CCS-MPC based on a feedforward ANN controlled VSI is described in [19]. Although a complex training method for the ANN is used to get the optimum voltage vector which is difficult in real-time, however the CCS MPC has a good performance in steady state operations [20].

This paper proposes a CCS MPC with sine pulse width modulation (SPWM) for better power quality. Inverter installation in an existing grid system is generally tied to several system factors. However, each inverter configuration must be independently programmed to minimize energy and time loss. Most of the research papers use three-phase control, which needs tuning of coefficients of three phases. This paper proposed an approach to optimize the controller setting for the VSI to achieve a plug-and-play feature in the MG. In this paper, a terminal voltage control method is used for the magnitude control of the voltage where a single variable needs to be controlled, which is more manageable and creates less burden on the controller. This method is friendly for the user, and no tuning arrangement of the controller is required here, unlike the PI

controllers [21], [22]. PSO is used in [19] to determine PI controller gains, but this technique may be lost in the suboptimal region. Therefore, a backtracking line search algorithm is proposed with PSO for better results in [23]. In this paper, a backtracking line search algorithm is used for optimized results by MPC. Moreover, in most research papers, inverter is modelled using RLC circuits neglecting the nonlinearity of semiconductor switches. This paper also includes the nonlinearity of switches in inverter modelling. Describing function method analysis of the modelled inverter guarantees stable operation. Moreover, a fault-resilient robust system is designed to overcome power interruption in the microgrid during the occurrence of a fault at the grid source.

To demonstrate the above-mentioned characteristics, this paper models a real-time distribution network in MATLAB/Simulink, following the loading pattern of the network, to demonstrate controller potential in terms of power quality. An existing 11kV feeder (Elachi feeder) from a 33/11 kV sub-station at Narendrapur, belonging to West Bengal state electricity and distribution company limited (WBSEDCL), India is studied, where voltage control is only through the on-load tap changers of the power transformer (PTR1, 2, 3). The absence of dynamic voltage control causes fluctuation in the industrial loads which is detrimental to the plant, machinery and production. The salient features of the proposed work are as follows:

- Terminal voltage magnitude method: The three-phase voltages are controlled using a single terminal voltage magnitude method in the proposed controller.
- The nonlinearity of the inverter: The Inverter has nonlinear dynamics, which research articles neglect to achieve simplicity. This paper takes care of the nonlinear behaviour of the inverter.
- Robustness: Resilient control action for the fault in the distribution feeder line and the external wires which connect the solar panel to the inverter are also taken care of to provide robustness to the MG.
- Plug and play feature: The proposed inverter control can be attached to any point of the MG. network.

The paper is organized as follows: i) Proposed method with system architecture using proposed controller design is detailed in section 2; ii) The theoretical basis of the proposed method is described in section 3; iii) The design aspect and control circuit for the robust fault-resilient microgrid is explained in section 4; and iv) Simulation results are presented in section 5, and the paper is concluded in section 6.

2. PROPOSED METHOD

The proposed control on the grid-tied PV inverter for plug-and-play operation is discussed in this section. The system architecture is modelled from a real-time system shown with blue dashed lines in Figure 1. The applied Simulink model is shown in the red dashed line where the inverter is installed.

2.1. System architecture

In this article, Elechi feeder of Narendrapur substation in West Bengal is modelled in MATLAB/Simulink. The architecture of the MG is depicted in Figure 1. It has two distinct portions. The red dotted line on the right-hand side indicates the architecture of the MG. The left-hand part, surrounded by green dotted lines, shows the 33/11 kV Narendrapur Substation of West Bengal State Electricity Distribution Company Limited (WBSEDCL). Sources of the substation are two incoming feeders (INC), 33 kV INC-1 (from Sonarpur) and 33 kV INC-2 (from Mahinagar). These feeders supply the 33 kV bus at Narendrapur and then further step down to 11 kV. This 11 kV bus is the source of the Elachi feeder. This is a mixed feeder with most industrial loading and some households. Table 1 reveals the load characteristic of this feeder system. Following the loading pattern, a system is modelled in MATLAB/Simulink. A 100 kVA, 11/0.433 kV distribution transformer is supplying microgrid loads. The loads are simulated with induction motors and resistive and inductive loads in Simulink. The system configuration block diagram in Figure 2 comprises the MG connected to the main grid. A microgrid may have several distributed energies resources (DERs) connected within it. Here a single inverter control is presented to illustrate the operation of the inverters within the microgrid. As the microgrid is spread over a small area, the IGBT based VSI with CCS-MPC control is assumed to be connected to the point of common coupling (PCC). Terminal voltage magnitude (V_t) is calculated from the three-phase voltages at the PCC end and fed back to the MPC. A second order closed-loop transfer function with an on-off nonlinearity has been found as a suitable model for the VSI system and used to train the ANN [24]. A non-linear autoregressive exogenous (NARX) series parallel based ANN is used to predict the plant output. The prediction horizon refers to the number of future control intervals the MPC controller evaluates by prediction at any instant. Optimization occurs based on the control horizon, but only the first variable, the modulation index (m), is applied to the system. Figure 3 shows the typical highest loading pattern of the year for the 11 kV Elachi feeder and Narendrapur 33/11 kV substation as the study time is the month of June. The loading pattern considered for simulation is from 23.00 hours of 06 June 2021 (day1) to 06.00 hours of 07 June 2021 (day2), as marked in Figure 3.

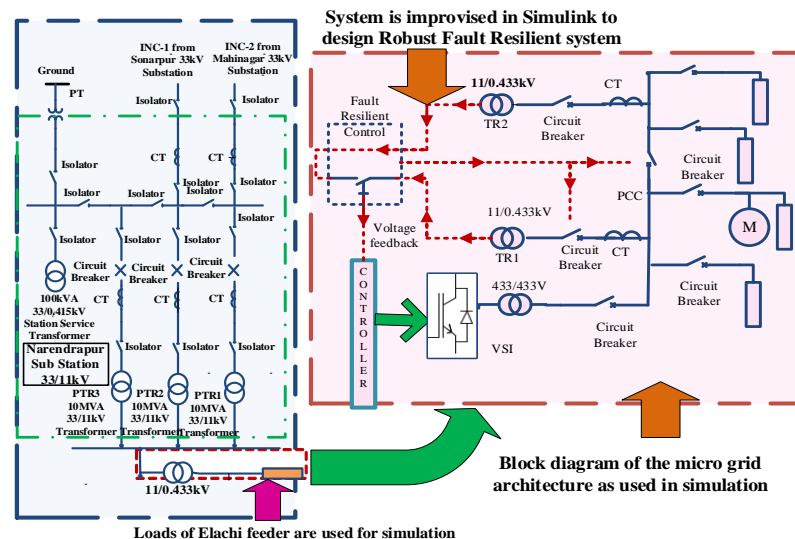


Figure 1. The architecture of the MG network

Table 1. Load pattern at 11 kV Elachi feeder, Narendrapur

Date	Time (hours)	Hourly loading of 11 kV Elachi feeder (A)	Set current (A)	Bus voltage (kV)	Ratio load
06 June 2021	23.00	250	300	10.9	0.833
07 June 2021	00.00	240		10.9	0.8
	01.00	218		10.9	0.727
	02.00	202		11.0	0.673
	03.00	186		11.1	0.62
	04.00	172		11.2	0.573
	05.00	156		11.3	0.52
	06.00	160		11.4	0.533

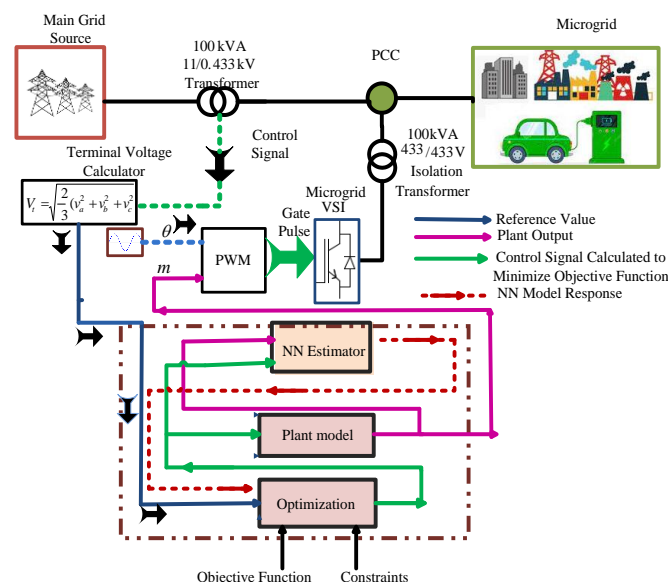


Figure 2. System configuration

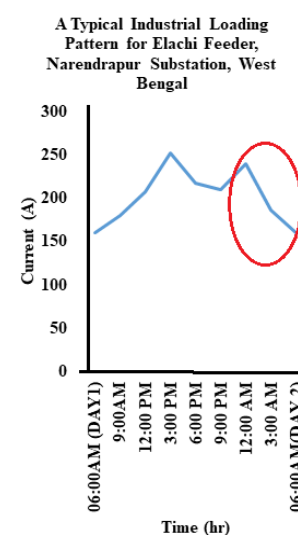


Figure 3. Load pattern of the feeder

2.2. Proposed controller design

A CCS-MPC is applied in this research article to maintain the voltage regulation of the ac bus. MPC has a wider aspect as a controller. CCS MPC provides fixed switching frequency and maintains good response in steady state operation. In the proposed control scheme, the ANN represents a plant model for output prediction by the MPC. NARX model in series-parallel architecture is used in this paper. Auto regressive

model is used to represent the time varying parameters of the power network as shown in Table 1. Auto regressive values predict future values from past observations. The proposed control avoids tuning of PI controllers in multiple loops. The nonlinearity of the semiconductor switches has also been adopted in the system model to minimize error. Describing function is applied for the stability of the designed nonlinear VSI model, which is a method for frequency response of nonlinear system. The nonlinear VSI model is illustrated in Figure 4. The nonlinearity is modelled using on-off, as shown in Figure 4(a), where v_o is the voltage coming out from the circuit, and v_e is the driving voltage of the semiconductor switch. The linear portion of the inverter is represented here as a 2nd order transfer function ($G(s)$). $G(s)$ and nonlinear describing function ($N_f(A, \omega)$) with on-off nonlinearity is shown in Figure 4(b).

The neural network model is developed as a time series model. The terminal voltage magnitude is used as input to the plant. The input and output from the plant are fed to the neural network. The plant model generates output following the step response of a 2nd order slightly underdamped system. The inverter model is discussed in the next section. The output from the plant transfer function with on-off nonlinearity block in series are simulated with normalized value of applied voltage. The output is considered as modulation index, m . Finally, the input voltage and m are applied to the neural network model. The ANN model is designed using a nonlinear auto-regressive exogenous series-parallel model [25]. This architecture is employed because the model is stable and a good predictor of time series value. Further, it has a purely feedforward construction. Input and target variables are set for training. Bus voltage at PCC and bus loading factor time series values are taken simulating the MG system for different loading condition. These are taken as input data. Target values are obtained from the inverter model as m . Now, ANN is trained first, and the performance as well as regression values are checked. The training process is repeated until the regression values for training, validation, and testing are all nearly equal to 1. After the training, the network is used for output prediction. ANN predicts the future value of m , which is then fed to the optimization block.

MPC optimizes the value of output based on the ANN system model. It minimizes the cost function over a receding horizon using the modelled output. This minimization of cost function demands optimization algorithm. Here it has been considered that the degree of optimization problem remains the same throughout different operating points and a linear adaptive MPC is implemented as it would be able to identify the single global optimum of the convex optimization issue.

2.2.1. Inverter model

The equivalent circuit of an inverter can be represented as an LC circuit, as shown in Figure 4(c), with v_x considered as step voltage [26]. A standard 2nd order transfer function is chosen to model the inverter. A standard second-order closed loop system transfer function, $G(s)$, is given as (1).

$$G(s) = \frac{k\omega_n^2}{s^2 + 2\zeta\omega_n s + \omega_n^2} \quad (1)$$

Where k = DC gain; ζ = damping ratio; ω_n = un-damped natural frequency of oscillation; RLC circuit can be modeled as 2nd order differential in (2).

$$L \frac{di}{dt} + Ri + \frac{1}{C} \int i dt = v_x \quad (2)$$

Where L = inductor value, R = resistance, C = the capacitance value, i = circuit current, and v_x = step voltage in the equivalent circuit shown in Figure 4(c). Thus, the transfer function (TF) is given as (3).

$$\therefore T.F = \frac{1/LC}{s^2 + sR/L + 1/LC} \quad (3)$$

Comparing it with (1),

$$\omega = \sqrt{1/LC} \text{ and } \zeta = (R/2)\sqrt{C/L}$$

the (1)-(3) are used in modeling the linear part of the inverter. Nonlinear dynamics of the inverter output voltage are described using the following describing function (DF), which implies the application of dead-time, hysteresis and relay [27]. It is a method for analyzing any nonlinear system with the best-suited linear time-invariant (LTI) function. Thus, using the nonlinearity as mentioned earlier, describing the function for the inverter is modeled as (4).

$$N_d(A, \omega) = \frac{4}{\pi} \frac{V_d}{A} \sqrt{1 - \left[\frac{r}{A}\right]^2} - j \frac{4}{\pi} \frac{rV_d}{A^2} \quad (4)$$

Where V_d denotes battery voltage, A is the peak value of sinusoidal current, r is the threshold voltage of semiconductor switch. In this work, threshold voltage of semiconductor switch is ignored in modeling for the sake of simplicity. Thus, the final describing function leads to (5).

$$N_f(A, \omega) \approx \frac{4 V_d}{\pi A} \quad (5)$$

The (4) leads to a model of an on-off nonlinearity. In Figure 5, Γ_G is the representation of the Nyquist plot of $G(s)$ while Γ_N is used for the polar plot of $\{-1/[N_f(A, \omega)]\}$. The (3) and (5) indicates the linear transfer function and nonlinear describing function of the modelled inverter respectively. Figure 5 presents the of stability analysis of inverter model using Nyquist plot for linear transfer function and polar plot for describing function. As Γ_G and Γ_N of the modeled inverter do not intersect therefore the modeled inverter design is stable [28]. It means any oscillation that may occur in the system output due to disturbance dies out and no sustained oscillation exists at a steady state. The objective of any feedback control system is to maintain the system goal, and it is done by measuring the output variable and permitting the actuating signal to achieve the desired system performance. The voltage at PCC is fed back to the control circuit of VSI. The three-phase instantaneous voltages are converted to the magnitude of terminal voltage, and the following transformation gives V_t :

$$V_t = \sqrt{(2/3)v_a^2 + v_b^2 + v_c^2} \quad (6)$$

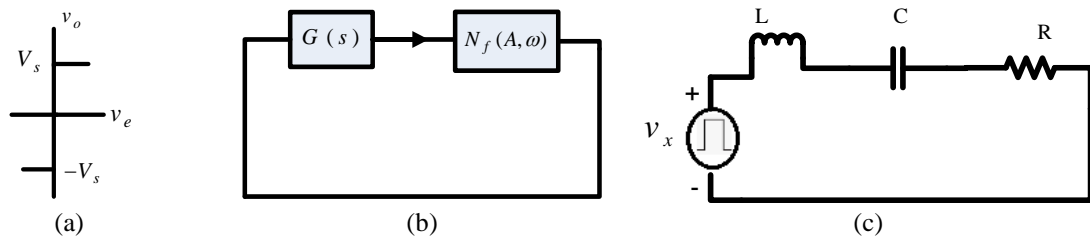


Figure 4. Inverter model with (a) on-off nonlinearity, (b) system structure represented by linear transfer function and nonlinear describing function, and (c) linear equivalent circuit of inverter

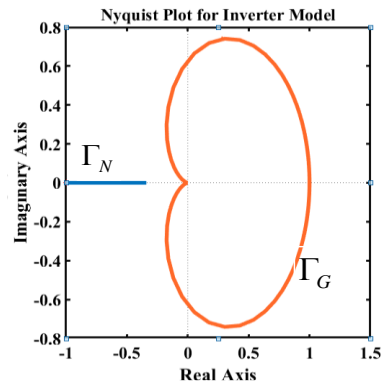


Figure 5. Stability analysis of inverter model using Nyquist plot describing function

3. THEORETICAL BASIS OF THE PROPOSED METHOD

3.1. Plant recognition

The prediction equation of NARX model with series-parallel structure as shown in Figure 6(a) is:

$$\hat{y} = f[u(k), u(k - d_1), u(k - d_2), \dots, y(k), y(k - d_1), y(k - d_2), \dots] \quad (7)$$

where u is the control inputs, d signifies the time delay, and y is the output from the plant model. After initializing the parameters as mentioned above, the neural network is ready for training.

This training process optimizes the network performance. mean square error (MSE) governs the performance function.

$$MSE = \frac{1}{N} \sum_{i=1}^N (e_i)^2 = \frac{1}{N} \sum_{i=1}^N (\hat{y} - y)^2 \quad (8)$$

Where e_i = error between the network output (\hat{y}) and target output (y). The neural network is trained in batch mode. Levenberg-Marquardt (LM) algorithm is used here for backpropagation training for the minimization of cost function $J(\theta)$ [29]. For any fitting problem, the aim is to minimize the error between output data and the fitting function. The rule for LM is as in (9).

$$\Delta\theta = (H + \mu I)^{-1} h_{lm} \quad (9)$$

Where h_{lm} is the gradient vector ($J^T e$), H is the approximated Hessian matrix (J^{TJ}), I is the identity matrix, and μ is the learning parameter. After repeated training, the regression response is shown in Figure 6(b). Mean normalization is applied to convert the input (u) and target data to be better applicable for training, as mentioned before (10).

$$u = u - M/s \quad (10)$$

Here M is the mean of all feature values, and s is the standard deviation. After training, validation is done using the validation data set.

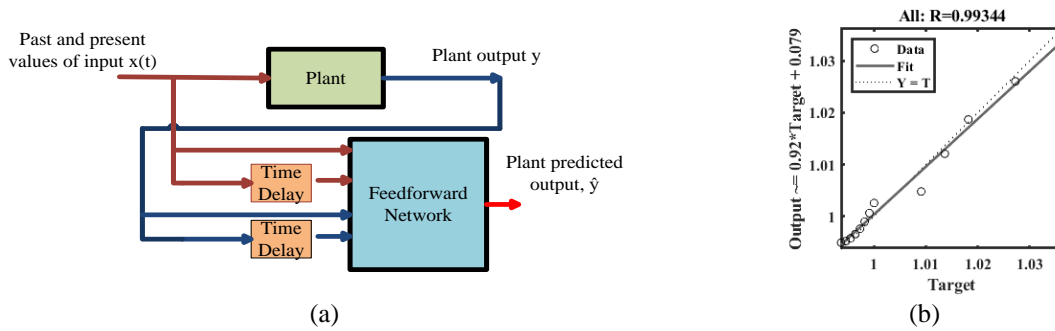


Figure 6. Series Parallel NARX model (a) structure and (b) regression response after training

3.2. Receding horizon control

Receding horizon control (RHC) is also known as moving horizon control (MHC). The principle of the receding horizon controller is shown in Figure 7. As per the principle of this technique, the future output is predicted over the future time step N , which is known as the future horizon. The current time, k , and current state x_k at k optimal control problem is solved over the future horizon, $[k, k+N-1]$ [30]. Though the whole future control trajectory is calculated, it only applies to the first-time step in the calculated optimal result. Next, the measure is taken at time $k+1$. This same procedure repeats itself in the next sampling instants over a fixed future horizon, i.e., between $[k+1, k+N]$ at the current state $[x_{k+1}]$. The optimization process determines the control signal to minimize the cost function, J , over the setout horizon.

$$J = \sum_{i=N_1}^{N_2} [W(k+i) - \hat{y}(k+i)]^2 + \rho \sum_{i=1}^{N_u} [u'(k+i-1) - u'(k+i-2)]^2 \quad (11)$$

Where N_1 , N_2 , N_u describes the horizons over which the tracking error and the control increments are evaluated, and u' describes the tentative control variable. W is the reference, and \hat{y} is the predicted output. The value of ρ determines the contribution of the sum of squares of the control increments on the performance index, J . The model predictive control performs an optimization procedure repeatedly to determine the best input condition within a specified horizon to meet the desired output response while maintaining the constraints. Here prediction horizon of $N_2 = 7$ and a control horizon of $N_u = 2$ with control weight $\rho = 0.05$ is used.

The controller action performs optimization over and over again as follows:

- a) Step 1: minimization of open-loop control

$$uN(x_0) = \arg \min JN(x_0, uN) \\ uN \in UN$$

subject to:

$$\begin{aligned}
J_N(x_0, u_N) &= \sum_{i=0}^{N-1} l(x_{uN}(i, x_0) - x_{ref}(i), u_N(x_0, i)) \\
x_{uN}(i+1, x_0) &= f(x_{uN}(i, x_0), u_N(x_0, i)) \forall i \in \mathfrak{I}_u \\
x_{uN}(0, x_0) &= x_0 \\
x_{uN}(i, x_0) &\in X \forall i \in \mathfrak{I}_x \\
u_{uN}(x_0, i) &\in U \forall i \in \mathfrak{I}_u
\end{aligned}$$

where time set $\mathfrak{I}_u = \{0, 1, \dots, N-1\}$; control function $u_N: \mathfrak{I}_u \rightarrow U$; state space is X
b) Step 2: solve for (11)

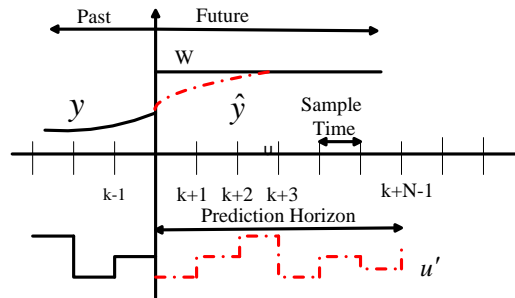


Figure 7. Receding horizon principle

3.3. Online optimizer

The optimization algorithm presented here uses a multilayer prescribed time horizon. The neural network reciprocates the plant dynamics, which has to be controlled. This ANN-based plant model estimates future responses based on control signals. An optimization routine is then set to optimize the control inputs for the original plant for effective output responses maintaining the constraints over the input and following the prescribed path while moving towards the reference set value. The cost function is differentiable in nature. The optimizer determines u' to minimize the cost function. Then the optimal input is fed to the plant. The computation of α_k is called the line search. The procedure for line search is as follows:

- i) Step I: choosing of initial state x_0 , putting $k = 0$
- ii) Step II: till convergence of x_k :
 - a) Search direction of ρ_k from x_k calculation considering

$$[g^k]^T \rho^k < 0 \text{ if } g^k \neq 0 \quad (12)$$

where g^k is Lipschitz continuous gradient

- b) Calculation of $\alpha_k > 0$ such that

$$f(x_k + \alpha_k \rho_k) < f^k \quad (13)$$

- c) Setting

$$x_{k+1} = x_k + \alpha_k \rho_k \quad (14)$$

However, the challenge here is to get a good α_k to avoid step lengths from becoming too long or too short. Therefore, a backtracking line search algorithm is applied in this proposed controller. Backtracking line search starts with a relatively larger step size but decreases the step size as required to obtain optimized target. This paper uses a search parameter of 0.1 for applying the backtracking line search algorithm to reach the Armijo-Goldstein inequality condition.

Backtracking line search algorithm

- i) Given $\alpha^{(init)} > 0$, let $\alpha_0 = \alpha^{(init)}$ and $l = 0$
- ii) Until $f(x_k + \alpha_l \rho_k) < f_k$
 - a) $\alpha_{l+1} = \tau \alpha_l$ where $\tau \in (0, 1)$
 - b) $l = l + 1$
- iii) Set $\alpha_k = \alpha_l$

4. ROBUST FAULT RESILIENT SYSTEM DESIGN

Robust fault-resilient system is implemented in the MG network for line-to-ground fault at the grid end and at the outdoor near the solar panel. The block diagram of the control circuit for the fault-immune system is shown in Figure 8. A fault-resilient system is designed to maintain power during a fault at the end of supply transformer. The inverter is connected at the PCC of the MG. network and maintains the voltage profile. A feedback loop between the source and inverter intimates the VSI of the required action. This feedback interrupts the fault at the grid source end as the circuit breaker disconnects the faulty section. This work includes a control approach to maintaining communication during link failure, as illustrated in Figure 8(a). Additional arrangement from the neighbourhood transformer of a parallel feeder is connected via a relay arrangement. If the fault occurs at the feeding source of the MG., the control signal from transformer T1, i.e., V_{T1} , becomes zero. This situation operates the relay, and neighbouring transformer T2 supplies the MG. Fault at exposed solar panel circuits and feeding wires may occur as it is placed outside. In this situation, the control circuit switches to the battery source for uninterrupted power, as shown in Figure 8(b).

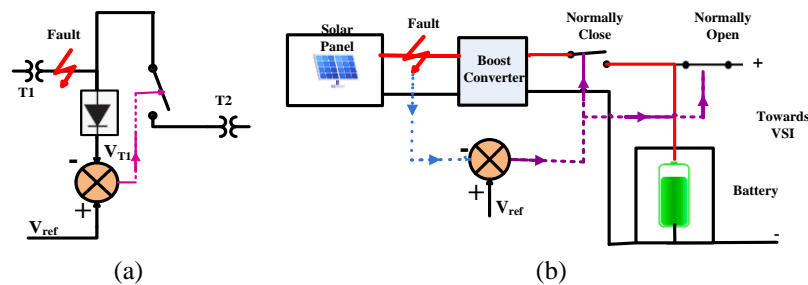


Figure 8. Fault resilient control circuit for (a) fault near grid source and (b) fault at environment exposed circuit of the solar panel

5. RESULTS AND DISCUSSION

This section describes the results in detail. Results are arranged in two subsections to justify the proposed method. The first section explains the inverter controller action with load variations, and the other section analyzes the arrangements during system faults.

5.1. Load variation

In this paper, the loading pattern of a distribution system is simulated, as mentioned earlier. The simulation parameters are mentioned in the Table 2 are for the reference. The condition of the simulated system with a change in the loading condition is shown in Figure 9. The variation of load in terms of active power is given in Figure 9(a). In the simulation, a 4 kW squirrel cage induction motor and a 2 kW resistive load gets disconnected at 1.2 sec and 1.5 sec, respectively. Figure 9(b) shows the three-phase voltages during the entire period with the solar-fed inverter connected to a microgrid. Figure 10 compares the terminal voltage profile with and without the inverter connected to the microgrid system. Figure 10(a) depicts that since the grid-connected microgrid operates initially at peak load conditions without any inverter attached at PCC, the voltage at PCC drops from the reference value (433 V). It has been mentioned initially that a real-time system is modelled in Simulink as a microgrid which has voltage control through only an online tap changer.

Therefore, during maximum loading conditions, the system is not able to maintain the voltage profile, and the voltage goes below the reference value. However, the inverter equipped with the proposed controller can instantly maintain the voltage profile at the reference value, supplying reactive power to the grid without any tuning process, as shown in Figure 10(b). The proposed ANN-MPC method controls the modulation index m . A phase-locked-loop (PLL) is used to create the phase angle ωt , m , and ωt is used for a 50 Hz sinusoidal signal. A 5 kHz triangular carrier signal is compared with the modulating signal for gate pulse generation for the VSI. Figure 11 describes the voltage profile of the PCC when an induction motor (IM) starts during peak load conditions with the inverter connected to the system. Figure 11(a) shows that an induction motor is switched on at 0.05 sec, but the PCC voltage before and after switching displays a satisfactory result, with the other loads connected at PCC remaining unaffected. Figure 11(b) shows the magnitude of terminal voltage (V_t) during and after the switching of the induction motor. It indicates that after a drop at the switching instant, the terminal voltage again attains the reference value within 0.1 sec. The modelled VSI is a 2nd order underdamped system which has overshoot in response. MPC controller is fast but susceptible to overshoot. However, an optimized model design and an appropriate number of control variables resulted in no overshoot in the simulation.

Table 2. Simulation parameters for the system improvised in the MATLAB/Simulink

Elements	Specifications
Grid system	
Source	11 kV rms (line-line), 50 Hz
Source parameters	$R_s = 0.8929 \Omega$, $L_s = 15.58 \text{ mH}$
Transformer	100 kVA, 11/0.433 kV delta/star, 3 phase
Line parameters	$R_L = 0.1 \Omega$, $L_L = 0.1 \mu\text{H}$
Microgrid system	
Source	PV module OC voltage: 36.3 V S.C. current: 7.84 A No. of PV strings: 30 Module/string: 12
Boost converter parameters	$L = 1 \text{ mH}$, $C = 33 \mu\text{F}$
Load	Varying from 22 kW to 16 kW
Interfacing impedance	$R_i = 1 \Omega$, $L_i = 0.1 \text{ H}$
Battery rating	1000 V, 300 Ah

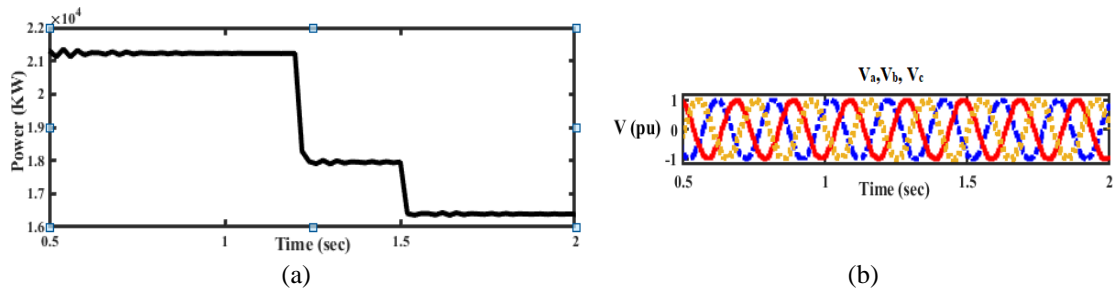
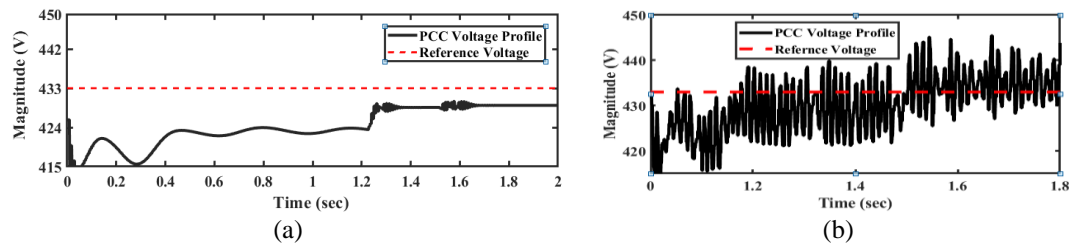
Figure 9. Modelled system under simulation with solar fed inverter connected with the MG network (a) load variation and (b) System line voltages V_a , V_b , V_c 

Figure 10. Simulated loading conditions (a) PCC voltage without controller and (b) PCC voltage with proposed controller

5.2. Fault resilient system

A temporary line-to-ground (L-G) fault is simulated near the grid source. Due to this fault, the circuit breaker operates and cuts off all three phases of the faulty section from the other part. The fault exists between 0.2 sec to 0.3 sec. Industrial processes experience huge losses due to sudden power interruptions. Therefore, an arrangement is proposed in which a fault near the AC source does not interrupt industrial processes in the MG. The control arrangement from the neighboring feeder transformer maintains the supply of MG during temporary power disruption at the source end. Figure 12 presents the voltage profile at PCC and source end during fault. The second diagram in Figure 12 clearly indicates that the feeder has no supply during the simulated fault between 0.2 sec to 0.3 sec, but the load connected at PCC is getting power. The DC bus voltage is shown in Figure 13. Output from the solar panel feeds the inverter during the daytime and charges the battery. If a power interruption occurs during the daytime, battery takes control to provide uninterrupted power. Figure 14 shows that due to a fault at 0.015 sec, the battery provides DC power for the VSI. The application of the inverter in the system deteriorates power quality, and voltage at PCC can be affected. However, in the proposed system, the PCC voltage shows total harmonic distortion (THD) within the limit. It indicates that the controller eliminates oscillations, thus reducing THD, indicating good quality power as in Figure 15.

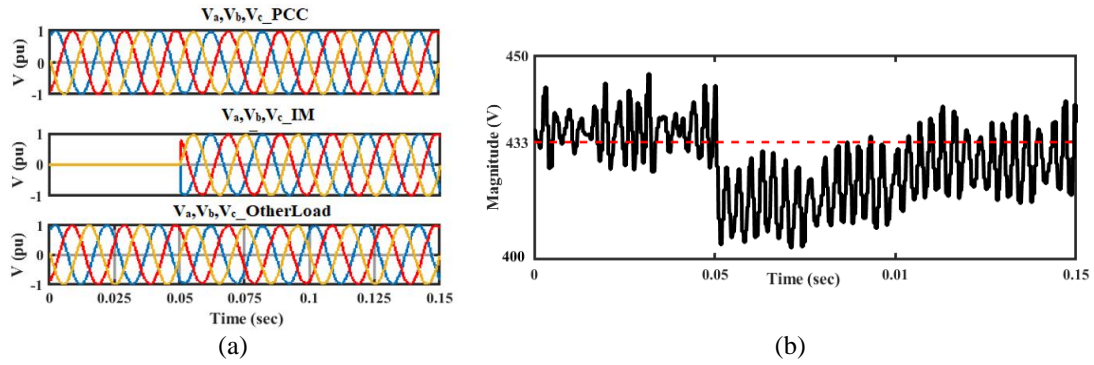


Figure 11. Voltage profile of PCC at the time of induction motor starting (a) voltage profile at the PCC during motor load switching at MG and (b) magnitude of terminal voltage at PCC during switching

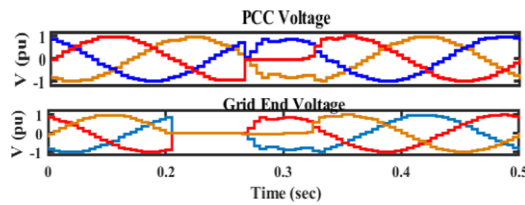


Figure 12. Voltage profile during L-G fault at grid source

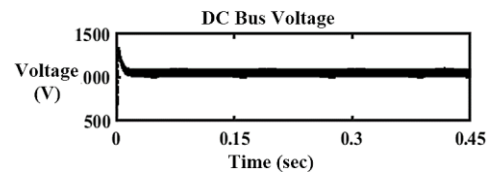


Figure 13. DC bus voltage of the inverter

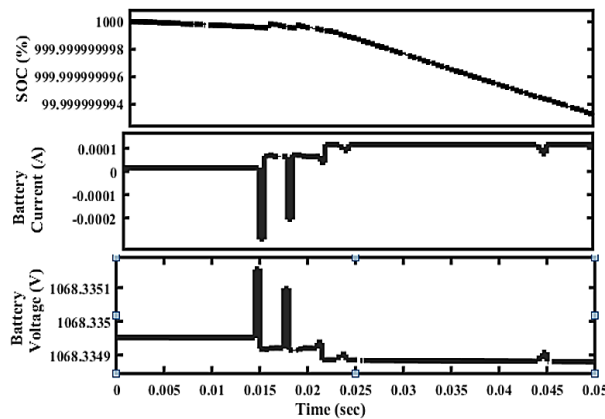


Figure 14. Battery profile during fault

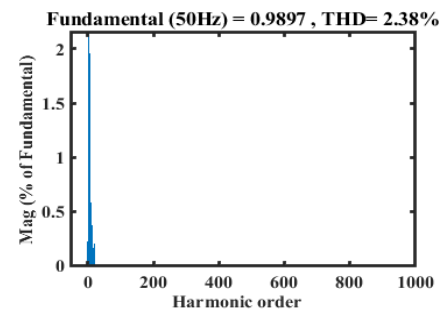


Figure 15. THD of 'V_a' at PCC

6. CONCLUSION

This paper proposes an ANN-CCS-MPC controlled inverter connected at PCC in a grid-connected MG to improve the ac bus voltage profile. This MG has been configured following the loading pattern of a real-life system. The proposed ANN-CCS-MPC controller regulates the inverter operation which improves the voltage profile by supplying the reactive power demanded by the system. The single variable magnitude of the terminal voltage technique in linear adaptive MPC avoids the interaction of multiple loops in conventional PI controllers or complex adaptive weight calculations of the three phases in other adaptive techniques for auto-configuration. The controller uses a nonlinear model of the inverter as the system and a series-parallel NARX model for the ANN for future output prediction. The advantage of the applied method is that it has small numbers of hardware and sensors compared to the three-phase variables for voltage regulation. The inverter model introduces on-off nonlinearity to include real-time semiconductor switch characteristics. The proposed control can introduce the VSI anywhere in the microgrid as plug-and play device. Simulation results of CCS-MPC control algorithm for the inverter establishes a satisfactory result. MPC tends to overshoot, but in this system, the VSI model and the number of control variables chosen restrict the overshoot. A fault-resilient arrangement is made in the microgrid to protect the loads connected to the source transformer in case a fault occurs at the source transformer. The control circuit automatically

switches the source feeder in case of a fault at the grid source end. The MG operation also takes care of a fault at the incoming lines from the solar panel to maintain constant power flow.

ACKNOWLEDGEMENTS

Authors acknowledge Meghnad Saha Institute of Technology, Department of Electrical Engineering to provide MATLAB software for this study.




REFERENCES

- [1] B. Blazic and I. Papic, "Improved D-StatCom control for operation with unbalanced currents and voltages," *IEEE Transactions on Power Delivery*, vol. 21, no. 1, pp. 225–233, Jan. 2006, doi: 10.1109/TPWRD.2005.859304.
- [2] M. G. M. Abdolrasol, M. A. Hannan, S. M. S. Hussain, and T. S. Ustun, "Optimal PI controller based PSO optimization for PV inverter using SPWM techniques," *Energy Reports*, vol. 8, pp. 1003–1011, Apr. 2022, doi: 10.1016/j.egy.2021.11.180.
- [3] O. M. Kamel, A. A. Z. Diab, T. D. Do, and M. A. Mossa, "A Novel Hybrid Ant Colony-Particle Swarm Optimization Techniques Based Tuning STATCOM for Grid Code Compliance," *IEEE Access*, vol. 8, pp. 41566–41587, 2020, doi: 10.1109/ACCESS.2020.2976828.
- [4] D. Venkatramanan and V. John, "A Reconfigurable Solar Photovoltaic Grid-Tied Inverter Architecture for Enhanced Energy Access in Backup Power Applications," *IEEE Transactions on Industrial Electronics*, vol. 67, no. 12, pp. 10531–10541, Dec. 2020, doi: 10.1109/TIE.2019.2960742.
- [5] Y. Gui, C. C. Chung, F. Blaabjerg and M. G. Taul, "Dynamic Extension Algorithm-Based Tracking Control of STATCOM Via Port-Controlled Hamiltonian System," in *IEEE Transactions on Industrial Informatics*, vol. 16, no. 8, pp. 5076–5087, Aug. 2020, doi: 10.1109/TII.2019.2957038.
- [6] F.-J. Lin, K.-C. Lu, T.-H. Ke, B.-H. Yang, and Y.-R. Chang, "Reactive Power Control of Three-Phase Grid-Connected PV System During Grid Faults Using Takagi–Sugeno–Kang Probabilistic Fuzzy Neural Network Control," *IEEE Transactions on Industrial Electronics*, vol. 62, no. 9, pp. 5516–5528, Sep. 2015, doi: 10.1109/TIE.2015.2407851.
- [7] N. Mahmud, A. Zahedi, and A. Mahmud, "A Cooperative Operation of Novel PV Inverter Control Scheme and Storage Energy Management System Based on ANFIS for Voltage Regulation of Grid-Tied PV System," *IEEE Transactions on Industrial Informatics*, vol. 13, no. 5, pp. 2657–2668, Oct. 2017, doi: 10.1109/TII.2017.2651111.
- [8] F. Benyamina, A. Benrabah, F. Khoucha, M. F. Zia, Y. Achour, and M. Benbouzid, "An augmented state observer-based sensorless control of grid-connected inverters under grid faults," *International Journal of Electrical Power & Energy Systems*, vol. 133, p. 107222, Dec. 2021, doi: 10.1016/j.ijepes.2021.107222.
- [9] R. Chilipi, N. Al Sayari, and J. Y. Alsawalhi, "Control of Single-Phase Solar Power Generation System With Universal Active Power Filter Capabilities Using Least Mean Mixed-Norm (LMMN)-Based Adaptive Filtering Method," *IEEE Transactions on Sustainable Energy*, vol. 11, no. 2, pp. 879–893, Apr. 2020, doi: 10.1109/TSTE.2019.2911852.
- [10] S. Huang, Q. Wu, W. Liao, G. Wu, X. Li, and J. Wei, "Adaptive Droop-Based Hierarchical Optimal Voltage Control Scheme for VSC-HVdc Connected Offshore Wind Farm," *IEEE Transactions on Industrial Informatics*, vol. 17, no. 12, pp. 8165–8176, Dec. 2021, doi: 10.1109/TII.2021.3065375.
- [11] M. Bouderbala, B. Bossoufi, H. A. Aroussi, M. Taoussi, and A. Lagrioui, "Novel deadbeat predictive control strategy for DFIG's back to back power converter," *International Journal of Power Electronics and Drive Systems (IJPEDS)*, vol. 13, no. 1, p. 139, Mar. 2022, doi: 10.11591/ijpeds.v13.i1.pp139-149.
- [12] J. Peng and M. Yao, "Overview of Predictive Control Technology for Permanent Magnet Synchronous Motor Systems," *Applied Sciences*, vol. 13, no. 10, p. 6255, May 2023, doi: 10.3390/app13106255.
- [13] I. M. Alsofyani and L. M. Halabi, "Unidirectional Finite Control Set-Predictive Torque Control of IPMSM Fed by Three-Level NPC Inverter with Simplified Voltage-Vector Lookup Table," *Electronics*, vol. 12, no. 1, p. 252, Jan. 2023, doi: 10.3390/electronics12010252.
- [14] N. Ahmed, Z. Soraya, and C. Abdelkader, "Model predictive control of high voltage direct current based on voltage source converter transmission system," *International Journal of Power Electronics and Drive Systems (IJPEDS)*, vol. 14, no. 1, p. 244, Mar. 2023, doi: 10.11591/ijpeds.v14.i1.pp244-255.
- [15] X. Chen, W. Wu, N. Gao, H. S.-H. Chung, M. Liserre, and F. Blaabjerg, "Finite Control Set Model Predictive Control for LCL-Filtered Grid-Tied Inverter With Minimum Sensors," *IEEE Transactions on Industrial Electronics*, vol. 67, no. 12, pp. 9980–9990, Dec. 2020, doi: 10.1109/TIE.2019.2962444.
- [16] J. C. U. Peña, L. P. Sampaio, M. A. G. de Brito, and C. A. Canesin, "RLC passive damped LCL single-phase voltage source inverter with capability to operate in grid-connected and islanded modes: design and control strategy," *Electrical Engineering*, vol. 102, no. 4, pp. 2509–2519, Dec. 2020, doi: 10.1007/s00202-020-01045-z.
- [17] F. Sebaaly, M. Sharifzadeh, H. Y. Kanaan, and K. Al-Haddad, "Multilevel Switching-Mode Operation of Finite-Set Model Predictive Control for Grid-Connected Packed E-Cell Inverter," *IEEE Transactions on Industrial Electronics*, vol. 68, no. 8, pp. 6992–7001, Aug. 2021, doi: 10.1109/TIE.2020.3003627.
- [18] J. Yang, Y. Liu, and R. Yan, "A Comparison of Finite Control Set and Continuous Control Set Model Predictive Control Schemes for Model Parameter Mismatch in Three-Phase APF," *Frontiers in Energy Research*, vol. 9, Aug. 2021, doi: 10.3389/fenrg.2021.727364.
- [19] I. S. Mohamed, S. Rovetta, T. D. Do, T. Dragicevic, and A. A. Z. Diab, "A Neural-Network-Based Model Predictive Control of Three-Phase Inverter With an Output LC Filter," *IEEE Access*, vol. 7, pp. 124737–124749, 2019, doi: 10.1109/ACCESS.2019.2938220.
- [20] R. P. Aguilera, P. Lezana, and D. E. Quevedo, "Switched Model Predictive Control for Improved Transient and Steady-State Performance," *IEEE Transactions on Industrial Informatics*, vol. 11, no. 4, pp. 968–977, 2015, doi: 10.1109/TII.2015.2449992.
- [21] A. K. Mishra, S. R. Das, P. K. Ray, R. K. Mallick, A. Mohanty, and D. K. Mishra, "PSO-GWO Optimized Fractional Order PID Based Hybrid Shunt Active Power Filter for Power Quality Improvements," *IEEE Access*, vol. 8, pp. 74497–74512, 2020, doi: 10.1109/ACCESS.2020.2988611.
- [22] M. S. Djebbar, A. Boukadoum, and A. Bouguerne, "Performances of a wind power system based on the doubly fed induction generator controlled by a multi-level inverter," *International Journal of Power Electronics and Drive Systems (IJPEDS)*, vol. 14, no. 1, p. 100, Mar. 2023, doi: 10.11591/ijpeds.v14.i1.pp100-110.




- [23] S. Nama, A. K. Saha, S. Chakraborty, A. H. Gandomi, and L. Abualigah, "Boosting particle swarm optimization by backtracking search algorithm for optimization problems," *Swarm and Evolutionary Computation*, vol. 79, p. 101304, Jun. 2023, doi: 10.1016/j.swevo.2023.101304.
- [24] M. Wang, X. Xu, Z. Yan, and H. Wang, "An online optimization method for extracting parameters of multi-parameter PV module model based on adaptive Levenberg-Marquardt algorithm," *Energy Conversion and Management*, vol. 245, p. 114611, Oct. 2021, doi: 10.1016/j.enconman.2021.114611.
- [25] Z. Boussaada, O. Curea, A. Remaci, H. Camblong, and N. Mrabet Bellaaj, "A Nonlinear Autoregressive Exogenous (NARX) Neural Network Model for the Prediction of the Daily Direct Solar Radiation," *Energies*, vol. 11, no. 3, p. 620, Mar. 2018, doi: 10.3390/en11030620.
- [26] P. K. W. P. K. W. Chan, H. S.-H. H. S. H. Chung, and S. Y. Y. Hui, "A Generalized Theory of Boundary Control for a Single-Phase Multilevel Inverter Using Second-Order Switching Surface," *IEEE Transactions on Power Electronics*, vol. 24, no. 10, pp. 2298–2313, Oct. 2009, doi: 10.1109/TPEL.2009.2028630.
- [27] M.-C. Kang, S.-H. Lee, and Y.-D. Yoon, "Compensation for inverter nonlinearity considering voltage drops and switching delays of each leg's switches," in *2016 IEEE Energy Conversion Congress and Exposition (ECCE)*, Sep. 2016, pp. 1–7, doi: 10.1109/ECCE.2016.7854946.
- [28] M. Vidyasagar, *Nonlinear Systems Analysis*. Society for Industrial and Applied Mathematics, 2002.
- [29] J. de J. Rubio, "Stability Analysis of the Modified Levenberg–Marquardt Algorithm for the Artificial Neural Network Training," *IEEE Transactions on Neural Networks and Learning Systems*, vol. 32, no. 8, pp. 3510–3524, Aug. 2021, doi: 10.1109/TNNLS.2020.3015200.
- [30] P. Grieder, M. Lüthi, P. A. Parrilo, and M. Morari, "Stability & feasibility of constrained receding horizon control," *European Control Conference, ECC 2003*, vol. 38, no. 10, pp. 701–706, 2003, doi: 10.23919/ecc.2003.7085038.

BIOGRAPHIES OF AUTHORS






Epsita Das    is working as Assistant Professor at Meghnad Saha Institute of Technology. She received her B. Tech degree from Netaji Subhash Engineering College, and M. Tech degree from University of Calcutta, Kolkata, India, in 2004, 2007 respectively. She is currently perusing for Ph.D. from Jadavpur University, Kolkata, India. Her research interest includes power quality issues in microgrid and smart grid. She can be contacted at email: epsita@msit.edu.in.



Ambarnath Banerji    is currently working as Professor at Electrical Engineering Department at Narula Institute of Technology. He worked as Principal of Polytechnic College 2004 to 2008 and then as Head of Department of Electrical Engineering at Meghnad Saha Institute of Technology. He became academic Chairman at Kingston Educational Institute. He has 22 years research experience in Industrial R&D on Process Control Instrumentation and around 21 years of academic research in power system, power quality, renewable energy, and microgrid. He received his Bachelor's degree in Electrical Engineering from University of Roorkee, India and Ph.D from Jadavpur University Kolkata, India. He is Fellow member IE(I) and Senior Member IEEE (USA). He can be contacted at email: ambarnathbanerji@gmail.com.



Sujit K. Biswas    was with the Department of Electrical Engineering, Jadavpur University, Kolkata. At present, he is with the Department of Electrical Engineering, St. Thomas College of Engineering and Technology, Kolkata, India. He was former professor and head Electrical Engineering Department, Jadavpur University, Kolkata, India. He received the BEE degree from Jadavpur University, Kolkata, in 1978, and the ME and Ph.D. degrees from the Indian Institute of Science, Bangalore, India, in 1980 and 1986, respectively, all in Electrical Engineering. He joined the Faculty of the Department of Electrical Engineering, Jadavpur University, in 1987. His fields of interest include static power conversion, electrical drives, power semiconductor applications, magnetics, and applied electronics. Fellow.I.E.(I), Fellow.I.E.T.E.(I), Sr. Member I.E.E.E.(USA). He can be contacted at email: sujit_biswas@hotmail.com.